Chinese Chemical Letters 35 (2024) 108696

Contents lists available at ScienceDirect

Chinese Chemical Letters

journal homepage: www.elsevier.com/locate/cclet

Crystal engineering regulation achieving inverse temperature symmetry breaking ferroelasticity in a cationic displacement type hybrid perovskite system

Na Wang, Wang Luo, Huaiyi Shen, Huakai Li, Zejiang Xu, Zhiyuan Yue, Chao Shi*, Hengyun Ye, Leping Miao*

Chaotic Matter Science Research Center, Department of Materials, Metallurgy and Chemistry, Jiangxi University of Science and Technology, Ganzhou 341000, China

ARTICLE INFO

Article history:
Received 24 April 2023
Revised 16 May 2023
Accepted 14 June 2023
Available online 19 June 2023

Keywords:
Organic-inorganic hybrid perovskite
Crystal engineering
Inverse temperature symmetry breaking
Displacement type phase transition
Ferroelasticity

ABSTRACT

Ferroelastic hybrid perovskite materials have been revealed the significance in the applications of switches, sensors, actuators, *etc*. However, it remains a challenge to design high-temperature ferroelastic to meet the requirements for the practical applications. Herein, we reported an one-dimensional organic-inorganic hybrid perovskites (OIHP) (3-methylpyrazolium)$CdCl_3$ (3-MBCC), which possesses a *mmmF2/m* ferroelastic phase transition at 263 K. Moreover, utilizing crystal engineering, we replace $-CH_3$ with $-NH_2$ and –H, which increases the intermolecular force between organic cations and inorganic frameworks. The phase transition temperature of (3-aminopyrazolium)$CdCl_3$ (3-ABCC), and (pyrazolium)$CdCl_3$ (BCC) increased by 73 K and 10 K, respectively. Particularly, BCC undergoes an unconventional inverse temperature symmetry breaking (ISTB) ferroelastic phase transition around 273 K. Differently, it transforms from a high symmetry low-temperature paraelastic phase (point group $2/m$) to a low symmetry high-temperature ferroelastic phase (point group $\bar{1}$) originating from the rare mechanism of displacement of organic cations phase transition. It means that crystal BCC retains in ferroelastic phase above 273 K until melting point (446 K). Furthermore, characteristic ferroelastic domain patterns on crystal BCC are confirmed with polarized optical microscopy. Our study enriches the molecular mechanism of ferroelastics in the family of organic-inorganic hybrids and opens up a new avenue for exploring high-temperature ferroic materials.

Crystal engineering is the comprehension of intermolecular interactions in the context of optimizing crystal performance, then utilizing such comprehension to design new solids with desired physical and chemical properties or to achieve significant performance improvements [1,2]. Nowadays, crystal engineering has developed into an effective strategy for efficiently constructing functional crystal materials. Simultaneously, it also has important theoretical significance for exploring the internal relationship between crystal microstructure and macroscopic properties.

As an important type of ferroicity, ferroelasticity is the mechanical equivalent of ferroelectricity or ferromagnetism. It exhibits an elastic hysteresis of mechanical force with a characteristic strain-stress hysteresis loop [3–5]. Ferroelastic materials possess two or more switchable spontaneous strain orientation states in the ferroelastic phase, which are widely applied to information processing, sensors, mechanical switches, *etc.* [6–10]. Inorganic perovskites have always been the mainstream of ferroelastic materials due to their excellent properties, such as $LaCoO_3$, $BiVO_4$, $BiFeO_3$, $Pb_3(PO_4)_2$ and $LaAlO_3$ [11–15]. However, their development is limited on account of the technical problems of high pressure, high temperature, and high energy consumption in the synthesis process. To meet the demands of low-cost, easy processing, environmentally friendly, and low density, sparked growing interest has been focused on molecular ferroelastics [16–19].

Recently, organic-inorganic hybrid perovskites (OIHP) have become a hot pot for developing molecular ferroelastic materials, owing to their excellent chemical diversity and structural tunability [20–23]. Among them, ABX_3 type hybrid perovskite $[CH_3NH_3]PbI_3$ is a classical ferroelastic material [24]. Nevertheless, most OIHP ferroelastics behave with a low phase transition temperature (T_c) and its ferroelastic state below T_c, implying a small practical working range of temperature. Since most of the structural phase transition (SPT) in the hybrid molecular system originates from order-disorder type requiring low motion energy barrier [25–30]. This

* Corresponding authors.
E-mail addresses: 15150517670@163.com (C. Shi), miaoleping@jxust.edu.cn (L. Miao).

https://doi.org/10.1016/j.cclet.2023.108696
1001-8417/

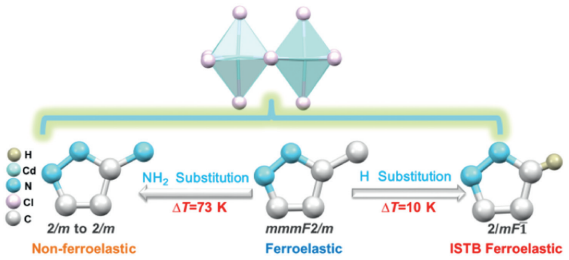

Scheme 1. Crystal engineering regulate strategy in 1D organic-inorganic hybrid perovskites 3-MBCC, 3-ABCC, and BCC.

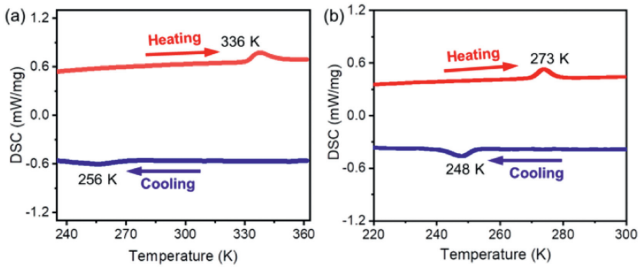

Fig. 1. The DSC curves of (a) 3-ABCC and (b) BCC.

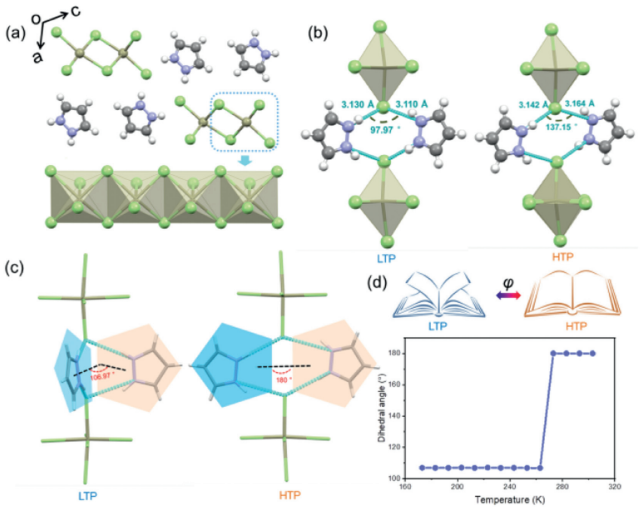

Fig. 2. (a) The molecular packing model and 1D inorganic chain of BCC in LTP 173 K. (b) The lengths of Cl-N and the angles of N-Cl-N are indicated in LTP 173 K and HTP 303 K. (c) Dihedral angle φ changes between the two groups HB planes in LTP 173 K and HTP 303 K. (d) Schematic diagram of ferroelastic phase transition mechanism (up) and temperature dependences of φ (down).

greatly restricted practical applications of molecular ferroelastic materials [31–33]. At present, the conventional method of enhancing the T_c of ferroic materials is mainly based on isotope effect, fluorine substitution, and strain engineering [34–38]. However, these methods are only aimed at some specific systems of compounds and without commonality. Consequently, to achieve high temperature molecular ferroelastic materials suitable for practical applications remains a huge challenge.

Structural phase transition can be mainly divided into two types: Order-disorder and displacive type in hybrid molecular systems [39,40]. As mentioned above, most of SPT in molecular hybrids are from the order-disorder motion of the intrinsic elements. These thermally driven phase transitions commonly involve a symmetry-breaking process of the low-temperature phase (LTP) with a lower symmetry and the high-temperature phase (HTP) with a higher symmetry [3,4]. These reveal that ferroicity only appears in the LTP, corresponding with aforesaid challenge. Thereby, abnormal symmetry-breaking process to achieve ferroicity retention in HTP will be an apromising choice. Fortunately, few cases report unconventional symmetry-breaking, *i.e.*, higher symmetries in the LTP and lower symmetries in the HTP, that is, inverse temperature symmetry breaking (ISTB) [41,42]. This provides an efficient avenue to obtain high temperature ferroelastic material. Currently, the known and only a small number of ISTB phase transitions are also derived from ordered disordered motion of the internal component [43,44]. Thus, non-order-disorder mechanism type ISTB ferroelastics will be extremely rare, equally, behaves high scientific value to explore high temperature molecular ferroelastic devices.

Herein, we reported three 1D ABX_3 OIHP compounds, (3-methylpyrazolium)$CdCl_3$ (3-MBCC), (3-aminopyrazolium) $CdCl_3$ (3-ABCC), and (pyrazolium)$CdCl_3$ (BCC). The latter two is designed based on crystal engineering theory (Scheme 1). 3-MBCC exhibits a *mmmF*2/m ferroelastic phase transition. After CH_3/NH_2-substitution, the phase transition temperature (T_p) increases markedly from 263 K in the former to 336 K in the latter. The big boost of T_p 73 K is difficult to achieve. This is attributed to the NH_2 substitution increasing the number of hydrogen bonds and enhancing the kinetic energy barrier. Furthermore, the T_c of BCC increased by 10 K after CH_3/H-substitution and exhibited rare ISTB ferroelasticity. Interestingly, its ISTB mechanism originates from the displacement of the organic cations which is different from the common order-disorder mechanism. These mean that BCC maintaining ferroelasticity in HTP until the melting point. This work opens a new vision to achieve high temperature ferroelastic materials and benefits for the application in molecular ferroelastic device.

Needle crystals of 3-MBCC, 3-ABCC and BCC were obtained by evaporating slowly from the saturated solution. Their phase purity was confirmed by powder X-ray diffraction (PXRD). The experimental PXRD patterns of three compounds were consistent with the simulated PXRD based on the single crystal structure information (Fig. S1 in Supporting information). Thermogravimetric analysis shows that 3-MBCC, 3-ABCC, and BCC are thermally stable up to 411, 349, and 446 K, respectively (Fig. S2 in Supporting information). Then the differential scanning calorimetry (DSC) measurement was used to preliminary study the reversible structural phase transition of three compounds. DSC curves of 3-MBCC display distinctly reversible endothermic and exothermic peaks around 263/193 K (Fig. S3 in Supporting information). This result reveals that 3-MBCC undergoes a reversible structural phase transition. When $-CH_3$ was replaced by $-NH_2$, BE, 3-ABCC, its DSC curves present a pair of reversible thermal anomalies around 336/256 K (Fig. 1a). Besides, after CH_3/H-substitution, DSC curves of BCC present a pair of reversible thermal anomalies at 273 (heating run) and 248 K (cooling run) (Fig. 1b). The phase transition temperature of 3-ABCC and BCC are 73 K and 10 K higher than that of 3-MBCC. It should be emphasized that the curves of three compounds exhibit obvious thermal hysteresis of 70, 80, and 25 K, separately, indicating first-order phase transition.

According to the DSC results, the variable-temperature single-crystal structures of 3-MBCC, 3-ABCC and BCC were collected by X-ray diffraction. Structurally, the three compounds all maintain the typical ABX_3 perovskite structure. Each Cd atom is octahedral coordinated by six bridging Cl atoms to form inorganic framework and then arranged in parallel 1D chain with the pyrazolyl cations (Figs. S4 and S7 in Supporting information, Fig. 2a). Owing to the free space between inorganic chains and the weak intermolecular interactions, it provides a great possibility for dynamic movement.

In LTP, 3-MBCC crystallizes in monoclinic space group of $P2_1/n$. The cell parameters are: $a = 3.8698(3)$ Å, $b = 20.7896(15)$ Å, $c = 11.0372(9)$ Å, $\alpha = \gamma = 90°$, $\beta = 91.404(7)°$, and $V = 887.694$ Å^3 (Table S1 in Supporting information). The Cd–Cl bond lengths

and the angles of Cl–Cd–Cl are 2.598 Å, 2.539 Å, 2.643 Å, 98.52°, 164.27°, 92.09°, respectively (Fig. S6a and Table S4 in Supporting information). The asymmetric unit contains hydrogen bonding (HB) linked 3-methylpyrazolium and a T-type inorganic anion $CdCl_3$. While in HTP, 3-MBCC adopts higher symmetry with orthorhombic space group *Pnma*. The cell parameters are: $a = 20.7942(13)$ Å, $b = 3.8854(3)$ Å, $c = 11.0659(6)$ Å, and $V = 894.056$ Å^3 (Table S1). The symmetry breaking of 3-MBCC LTP-HTP transition changes from monoclinic to an orthorhombic point group. It indicates that 3-MBCC may be a ferroelastic crystal with the notation of *mmmF2/m* based on Aizu's classification. At this time, Cd-Cl bond length and the angles of Cl–Cd–Cl was weakly changed (Fig. S6b and Table S4 in Supporting information). Intriguingly, in HTP, the two 3-methylpyrazoliums are still arranged in parallel, with the spacing between the two planes decreasing from 2.486 Å to 1.943 Å (Figs. S5c and d in Supporting information). Moreover, the methyl on the cation exhibits a slightly disordered state. Accordingly, the reversible SPT of 3-MBCC is derived from the displacement and order-disorder motion of cations.

Similarly, after $-CH_3/-NH_2$-substitution, 3-ABCC also crystallizes in $P2_1/n$ space group, with cell parameters of $a = 11.5189$ (4) Å, $b = 3.8254(2)$ Å, $c = 19.4163(6)$ Å, $\alpha = \gamma = 90°$, $\beta = 96.211$ (3)°, and $V = 850.546$ Å^3 (Table S2 in Supporting information). The Cd–Cl bond lengths are 2.581, 2.532, and 2.716 Å, respectively. And the angles of Cl–Cd–Cl are 100.15, 171.35, and 88.27° (Fig. S9a and Table S5 in Supporting information). Different from 3-MBCC, 3-ABCC adopts same space group $P2_1/n$ in HTP with a changed cell parameter: $a = 12.1033(5)$ Å, $b = 3.88532(17)$ Å, $c = 18.2173(9)$ Å, $\alpha = \gamma = 90°$, $\beta = 90.396(4)°$, $V = 856.652$ Å^3, which indicates an isomorphic phase transition (Table S2). The Cd–Cl bond lengths changes to 2.613, 2.493, and 2.613 Å, and the angles change to 98.43°, 166.05°, and 92.41° (Fig. S9b and Table S5 in Supporting information). More importantly, 3-aminopyrazolium and the Cd_2Cl_6 display obvious HB interactions. The distances of hydrogen bond N-H···Cl are 3.219 and 3.157 Å, and the hydrogen bond angles are 131.89° at 193 K. While heating to 323 K, the N-H···Cl length changes to 3.197 and 3.298 Å, same time, the HB angles decrease to 120.56° (Table S8 in Supporting information). The 11° change of the HB angles reveals the displacement of 3-aminopyrazolium based on the inorganic framework. The dihedral angle formed by the plane of two pyrazole cations changed from 180° to 178.65° (Fig. S8b in Supporting information). It is worth noting that the displacement of organic cations and the twist of the inorganic frameworks are the molecular origin of the phase transition. This kind of molecular mechanism of phase transition is extremely rare in hybrid systems due to most of them are order-disorder type [45–47].

After $-CH_3/-H$-substitution, BCC crystallizes in the monoclinic space group of *I2/a* (point group 2/*m*). The cell parameters are $a = 21.3889(12)$ Å, $b = 3.86570(10)$ Å, $c = 21.0474(11)$ Å, $\alpha = \gamma = 90°$, $\beta = 114.636(7)°$, and $V = 1581.86$ Å^3 (Table S3 in Supporting information). While in HTP, at 303 K, it adopts a lower symmetry with a triclinic crystal system and $P\bar{1}$ space group (point group $\bar{1}$) with the cell parameters: $a = 3.8845(2)$ Å, $b = 10.4180(6)$ Å, $c = 10.9984(6)$ Å, $\alpha = 65.969(6)°$, $\beta = 79.876(4)°$, $\gamma = 88.896(5)°$, and $V = 399.505$ Å^3 (Table S3). It presents that the symmetry of BCC reduces upon heating. For the mono crystal structures of BCC, in LTP at 173 K, in which the Cd–Cl bond lengths are 2.528, 2.598, and 2.644 Å, respectively. And the angles of Cl–Cd–Cl are 92.51°, 92.65°, and 170.59° (Fig. S11a and Table S6 in Supporting information). When in HTP at 303 K, the Cd–Cl bond lengths changes to 2.518, 2.607, and 2.654 Å, and the angles change to 91.15°, 91.91°, and 171.64° (Fig. S11b and Table S6 in Supporting information). The distances of hydrogen bond N-H···Cl are 3.110 and 3.130 Å, and the hydrogen bond angles are 97.91° at 173 K (Fig. 2b and Table S9 in Supporting information). While heating to 303 K, the N-H···Cl length increases to 3.142 and 3.164 Å, same time, the HB angles

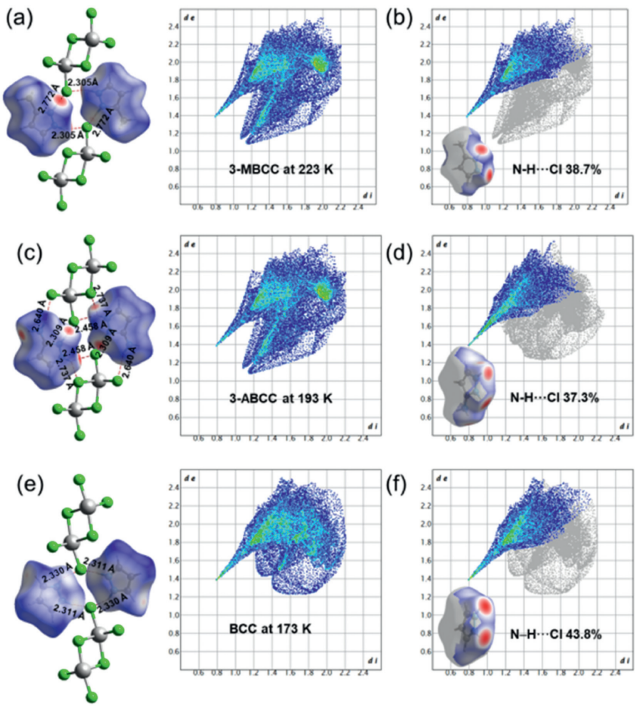

Fig. 3. (a, b) The HB length between Cl and H aotoms, visualization map of the distribution of the interactions and the 2D fingerprint plots of 3-MBCC in LTP at 223 K, (c, d) 3-ABCC in LTP at 193 K, and (e, f) BCC in LTP 173 K.

largely increase to 137.15° (Fig. 2b and Table S9). Likewise, the significant change in HB angles of 40° also indicates the displacement of pyrazolium based on the inorganic framework. The direct embodiment is the dihedral angle (φ) between the two group HB plane changes from about 107° (in LTP 173 K) to 180° (in HTP 303 K) (Fig. 2c). Besides, the φ shows a step like change around the T_c. The huge change of the φ checks the displacement of pyrazolium and like a half-open book changed to fully open (Fig. 2d and Table S10 in Supporting information). These results verify the SPT of BCC.

To understand N-H-Cl coordination bonds (CBs) generating intermolecular interactions between the cations and inorganic formworks, the visualization map of the distribution of the interaction was obtained by Hirshfeld surface analysis [48,49]. At 223 K, the Hirshfeld surface of 3-MBCC is dominated by blue and white regions, the red areas indicate strong molecular hydrogen bonding interaction [H···Cl]. The 2D fingerprint plots showing [H···Cl] interaction is 38.7% (Figs. 3a and b). Unfortunately, due to the slightly disordered state in HTP, Hirshfeld surface analysis cannot be performed. As for 3-ABCC, the [H···Cl] interaction is 37.3% in LTP at 193 K, while enhanced in HTP at 353 K, reaching 40% (Figs. 3c and d, Fig. S12 in Supporting information). For BCC, the [H···Cl] interaction is 43.8% in LTP and slightly enhanced to 44.3% in HTP (Figs. 3e and f, Fig. S13 in Supporting information). Therefore, it is lucid that the displacement of the cations indeed changes the spacing between H and Cl atoms, increasing the number of hydrogen bonds and enhancing the interaction between the cation and the inorganic framework. Additionally, compared with 3-MBCC, BCC shortens the length of hydrogen bonds and 3-ABCC increases the number of hydrogen bonds due to the presence of amino groups. These increase the motional energy barrier of the cations and anions, and eventually leading to a substantial increment in the T_c.

The macroscopic dielectric response is sensitive to the changes of microcosmic dipole orientation in molecular materials. In phase-transition compounds, the reversible structural phase transitions

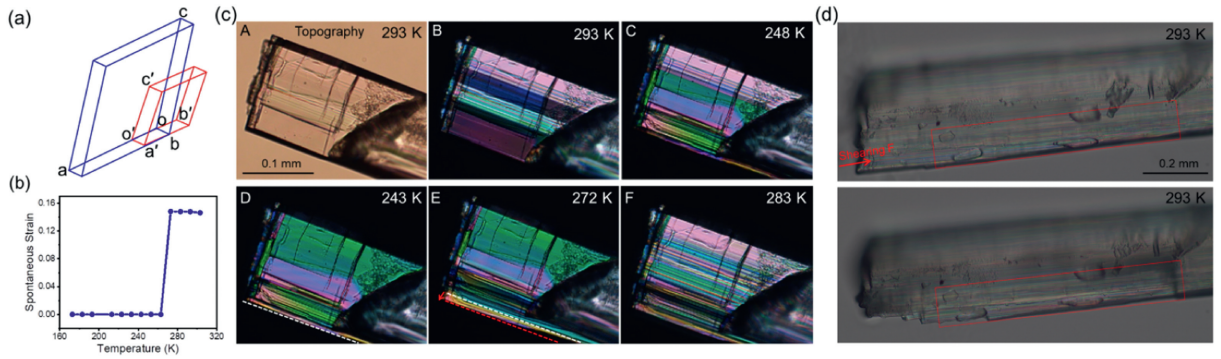

Fig. 4. (a) The unit cell of BCC at LTP and HTP. (b) Temperature-dependent ferroelastic spontaneous strain ε_s. (c) The ferroelastic domain walls evalution of BBC, natural optical microscope images for (A) single crystal of BCC, (B-F) evolutions of the ferroelastic domain structure for BCC in the cooling-heating runs, (d) ferroelastic domain structure changes (in red box) upon shearing stress on BBC mono crystal at 293 K.

are usually accompanied by dielectric anomalies around the phase transition point. Therefore, the dielectric response can verify the occurrence of structural phase transition to some extent. Here, we recorded the temperature dependence of dielectric constants (the real part (ε') of BCC in a heating-cooling cycle mode. The dielectric constant curve of BCC displays a large step-like dielectric anomaly at 100 kHz, confirming that BCC undergoes a phase transition (Fig. S14a in Supporting information). Moreover, the transition temperature of the dielectric anomaly of BCC was about 270 K in the heating cycle, which consistent with the DSC measurement result. In addition, the values of ε' decrease with increasing frequency (0.5, 1, 10, 100 kHz). This indicates that the dielectric constant of BCC is frequency dependent (Fig. S14b in Supporting information). The transition of high (switch ON) and low dielectric state (switch OFF) was performed to study the switchable dielectric feature of BCC. The results show that BCC undergoes a rapid dielectric transition from HDS to LDS in the vicinity of T_c. Besides, compared to the initial value, the intensity of the dielectric signals hardly attenuated over several heating-cooling cycles, which proves that the dielectric switches of BCC have good fatigue resistance (Fig. S14c in Supporting information). Therefore, BCC is a candidate material with great potential for stimuli-responsive electronic switching material.

As a truth, BCC undergoes a monoclinal-triclinic transition during the changing process from LTP to HTP. This means BCC adopts high symmetry in HTP and lower symmetry in LTP. This abnormal ISTB is few in the hybrid molecular system. Although previous work based on hybrids reported the ISTB mechanism of the SPT, almost all of them derived from the order-disorder, rare the conformational reversal [28,50–51]. The different is that the ISTB of BCC originates from the displacement of the organic cations. The monoclinal-triclinic transition of BCC belongs to ferroelastic transition with the Aizu notation of $2/mF\bar{1}$. The space group $I2/a$ in LTP belongs to the point group C_{2h} ($2/m$) with four symmetry elements (E, C_2, i, and σ_h), and the HTP space group $P\bar{1}$ with two symmetry elements (E, and i), a subgroup of C_i. This is an obvious group-subgroup relationship between LTP and HTP. Thus, the symmetry reduction presents in the comparison of the unit cell of LTP and HTP (Fig. 4a). Further, the theoretical calculation of ferroelastic spontaneous strain components is performed by the lattice parameters [52,53]. In theory, the spontaneous strain tensors for domains S_1 and S_2 are shown as follows:

$$\varepsilon_s(s_1) = \begin{bmatrix} 0 & \varepsilon_{12} & 0 \\ \varepsilon_{12} & 0 & \varepsilon_{23} \\ 0 & \varepsilon_{23} & 0 \end{bmatrix} \text{and } \varepsilon_s(s_2) = \begin{bmatrix} 0 & -\varepsilon_{12} & 0 \\ \varepsilon_{12} & 0 & -\varepsilon_{23} \\ 0 & -\varepsilon_{23} & 0 \end{bmatrix} \quad (1)$$

The detailed calculated methods and results of strain tensors ε_{12} and ε_{23} can be seen in the supporting information (Supporting information). So the spontaneous strain $\varepsilon_s = \sqrt{2\varepsilon_{12}^2 + 2\varepsilon_{23}^2}$ with a value of 0.1479 at 293 K. The temperature-dependent spontaneous strain ε_s show a step change from zero value in the LTP to 0.1482 above 273 K in the HTP (Fig. 4b and Tables S11–S13 in Supporting information). This value of spontaneous strain is larger than that of most organic-inorganic hybrids, and comparable to the reported hybrid ferroelastics with large spontaneous strains [19,29,31,40]. This result of microscopic order parameter (ε_s) also can confirm the ITSB ferroelastic phase transition.

Ferroelastic domains with different orientations show different birefringence phenomena under orthogonally polarized light, which manifested as the light and dark patterns of the ferroelastic domains. Meanwhile, the ferroelastic domains of crystals can evolve under appropriate stress or thermal stimulation. Thus, the evolution of ferroelastic domain structure can be visualized by using polarized optical microscope. Crystal topography observed without polarized light was uncorrelated with ferroelastic domains (Fig. 4c(A)). As shown in Fig. 4c(B), crystal BCC presents bright, distinct and stable ferroelastic domain structures under polarized light at 293 K. As the temperature cooling to 248 K, part of the ferroelastic domain disappeared and with changes in bulk crystal shape. When cooling to 243 K, the ferroelastic domain disappeared completely (Fig. 4c(C, D), Movie 1 in Supporting information). Further, a heating process was done. At 272 K, the ferroelastic phase transition (FPT) just beginning, we observed that the crystal expanded to the lower left (Fig. 4c(E)). Until 283 K, more numerous and stronger ferroelastic domains were re-observed. At the same time, the lower left extension of the macrocrystal returned to the original position (Fig. 4c(D, F), Movie 1). The change of ferroelastic domain under stress stimulation is the core evidence of ferroelasticity. Therefore, a test for observing ferroelastic domain changes under stress stimulation was performed at 293 K. Upon applying little stress, the domain wells show obvious changes in the red wireframe area (Fig. 4d). Simultaneously, we observed the bulk single crystal of BCC exhibited a transient twisting behavior during the cooling-heating cycles (Movie 2 in Supporting information). The visual changes of switching or movement behavior of the twin boundaries demonstrate the real ISTB ferroelasticity of BCC. Besides, the recorded twisting, expanding or moving of the bulk mono crystal of BCC during FPT may reveal the large spontaneous strain corresponding to the theoretical calculated value. The excellent ISTB ferroelastic performances prove BCC behaving more possibilities for the application in driver devices.

In summary, we constructed three 1D organic–inorganic hybrid perovskite compounds based on crystal engineering regulation. More importantly, it not only achieved a significant increase of phase transition temperature 73 K but also achieved high-temperature ferroelasticity. Remarkably, 3-MBCC, 3-ABCC and BCC

are rare displacement type hybrid phase transition materials that the molecular mechanism is derived from organic cation displacement. Additionally, the FPT of BCC is also accompanied by an unusual ISTB, meaning that crystal BCC retains in ferroelastic phase above T_c (273 K) until melting point (446 K). Moreover, BCC exhibits large spontaneous strain (0.1479) and excellent ferroelastic properties. Consequently, this work enriches the molecular mechanism of FPT and provides a new vision to achieve high temperature ferroelasticity which is beneficial to the applications in actuator devices.

Declaration of competing interest

The authors declare that they have no known competing financial interests or personal relationships that could have appeared to influence the work reported in this paper.

Acknowledgments

C. Shi acknowledges the support from the National Natural Science Foundation of China (No. 22175079). L.P. Miao acknowledges the support from the National Natural Science Foundation of China (No. 22205087) and the Open Project Program of Jiangxi Provincial Key Laboratory of Functional Molecular Materials Chemistry, Jiangxi University of Science and Technology (No. 20212BCD42018). H.Y. Ye acknowledges the National Natural Science Foundation of China (No. 22275075), Natural Science Foundation of Jiangxi Province (Nos. 20204BCJ22015 and 20202ACBL203001).

Supplementary materials

Supplementary material associated with this article can be found, in the online version, at doi:10.1016/j.cclet.2023.108696.

References

[1] G.R. Desiraju, The Design of Organic Solids, Elsevier, Amsterdam, 1989.
[2] A.D. Bond, CrystEngComm 14 (2012) 2363–2366.
[3] F. Jona, G. Shirane, Ferroelectric Crystals, Dover Publications Inc., New York, 1993.
[4] E.K.H. Salje, Annu. Rev. Mater. Res. 42 (2012) 265–283.
[5] J. Erhart, Phase Transit. 77 (2004) 989–1074.
[6] N. Balke, S. Choudhury, S. Jesse, et al., Nat. Nanotech. (2009) 868–875.
[7] P. Gao, J. Britson, C.T. Nelson, et al., Nat. Commun. 5 (2014) 4801.
[8] R.G. Xiong, S.Q. Lu, Z.X. Zhang, et al., Angew. Chem. Int. Ed. 59 (2020) 9574–9578.
[9] M.D. Hollingsworth, M.L. Peterson, K.L. Pate, et al., J. Am. Chem. Soc. 124 (2002) 2094–2095.
[10] A.I. Khan, X. Marti, C. Serrao, et al., Nano. Lett. 15 (2015) 2229–2234.
[11] E.J. Guo, R. Desautels, D. Keavney, et al., Sci. Adv. 5 (2019) eaav5050.
[12] H. Yokota, S. Matsumoto, E.K.H. Salje, et al., Phys. Rev. B 98 (2018) 104105.
[13] N. Balke, S. Choudhury, S. Jesse, et al., Nat. Nanotech. 4 (2009) 868–875.
[14] C. Hill, M.C. Weber, J. Lehmann, et al., APL Mater. 8 (2020) 081108.
[15] H. Yokota, S. Niki, R. Haumont, et al., AIP Adv. 7 (2017) 085315.
[16] M. Moskwa, E. Ganczar, P. Sobieszczyk, et al., J. Phys. Chem. C 124 (2020) 18209–18218.
[17] Z. Sun, X. Wang, J. Luo, et al., J. Mater. Chem. C 1 (2013) 2561–2567.
[18] H.Y. Zhang, C.L. Hu, Z.B. Hu, et al., J. Am. Chem. Soc. 142 (2020) 3240–3245.
[19] W. Yuan, Y. Zeng, Y.Y. Tan, et al., Chem. Commun. 55 (2019) 8983–8986.
[20] L. Lu, X. Pan, J. Luo, et al., Chem. Eur. J. 26 (2020) 16975–16984.
[21] Q. Xu, L. Ye, R.M. Liao, et al., Chem. Eur. J. 28 (2022) e202103913.
[22] X. Zhang, L. Li, Z. Sun, et al., Chem. Soc. Rev. 48 (2019) 517–539.
[23] R. Jakubas, M. Rok, K. Mencel, et al., Inorg. Chem. Front. 7 (2020) 2107–2128.
[24] Y. Liu, L. Collins, R. Proksch, et al., Nat. Mater. 1 (2018) 1013–1019.
[25] E. Strelcov, Q. Dong, T. Li, et al., Sci. Adv. 3 (2017) e1602165.
[26] L. Zhou, R.X. Li, P.P. Shi, et al., Inorg. Chem. 59 (2020) 18174–18180.
[27] X.Q. Huang, H. Zhang, F. Wang, et al., J. Phys. Chem. Lett. 12 (2021) 5221–5227.
[28] D.X. Liu, X.X. Chen, Z.M. Ye, et al., Sci. China Mater. 65 (2022) 263–267.
[29] H.Y. Zhang, Z.X. Zhang, X.J. Song, et al., J. Am. Chem. Soc. 142 (2020) 20208–20215.
[30] Y.Y. Tang, Y. Ai, W.Q. Liao, et al., Adv. Mater. 31 (2019) 1902163.
[31] X.Q. Xu, H. Zhang, X.Q. Huang, et al., Inorg. Chem. Front. 8 (2021) 1197–1204.
[32] Z.X. Wang, Y. Zhang, Y.Y. Tang, et al., J. Am. Chem. Soc. 141 (2019) 4372–4378.
[33] C.F. Wang, H. Li, M.G. Li, et al., Adv. Funct. Mater. 31 (2021) 2009457.
[34] M. Itoh, R. Wang, Y. Inaguma, et al., Phys. Rev. Lett. 82 (1999) 3540.
[35] K. Chang, J.W. Liu, H.C. Lin, et al., Science 353 (2016) 274–278.
[36] Y. Ai, H.P. Lv, Z.X. Wang, et al., Trends Chem. 3 (2021) 1088–1099.
[37] B.D. Liang, T. Jin, L.P. Miao, et al., Chin. Chem. Lett. 33 (2022) 1422–1424.
[38] S. Koval, J. Kohanoff, J. Lasave, et al., Phys. Rev. B 71 (2005) 184102.
[39] Q.R. Meng, W.J. Xu, W.H. Hu, et al., Chem. Commun. 57 (2021) 6292–6295.
[40] X. Zheng, L. Zhou, P.P. Shi, et al., Chem. Commun. 53 (2017) 7756–7759.
[41] S. Weinberg, Phys. Rev. D 9 (1974) 3357–3378.
[42] M. Szafranski, Cryst. Growth Des. 16 (2016) 3771–3776.
[43] P. Szklarz, A. Ingram, Z. Czapla, et al., Phase Trans. 90 (2017) 610–617.
[44] A. Ingram, S. Wacke, Z. Czapla, et al., Phase Trans. 92 (2019) 467–474.
[45] M.M. Zhao, L. Zhou, P.P. Shi, et al., Chem. Eur. J. 25 (2019) 6447–6454.
[46] S.N. Cheng, K. Ding, T. Zhang, et al., Chem. Eur. J. 27 (2021) 17655–17659.
[47] Y.P. Gong, X.X. Chen, B.Q. Zhao, et al., Chin. Chem. Lett. 34 (2023) 108282.
[48] M.A. Spackman, CrystEngComm. 4 (2002) 378–392.
[49] M.A. Spackman, D. Jayatilaka, CrystEngComm. 11 (2009) 19–32.
[50] L.P. Miao, L.L. Chu, X.B. Han, et al., Inorg. Chem. Front. 8 (2021) 2809–2816.
[51] B.Q. Zhao, X.X. Chen, H. Ye, et al., Chem. Sci. 14 (2023) 5965–5973.
[52] K. Aizu, J. Phys. Soc. Jpn. 28 (1970) 706.
[53] L.T. Li, C.X. Ji, Y.X. Sun, et al., Inorg. Chem. Front. 9 (2022) 1380–1385.